

# Preparation of cuttlefish ink-porphyrin nanoconjugates and its application in photodynamic-photothermal synergistic treatment of tumor cells

Wei Wang<sup>1,†</sup>, Yuting Zhang<sup>1,†</sup>, Yan Li<sup>1</sup>, Yuzi Huang<sup>1</sup>, Shuzhang Xiao<sup>1,\*</sup>, Wenquan Huang<sup>2,\*</sup>, Peng Geng<sup>1,3,\*</sup>

<sup>1</sup> College of Materials and Chemical Engineering, China Three Gorges University, Yichang 443002, China

<sup>2</sup> College of Medicine and Health Science, China Three Gorges University, Yichang 443002, China

<sup>3</sup> Hubei Three Gorges Laboratory, Yichang 443007, China

\* **Corresponding authors:** Shuzhang Xiao, [shuzhangxiao@ctgu.edu.cn](mailto:shuzhangxiao@ctgu.edu.cn); Wenquan Huang, [huangwenquan@ctgu.edu.cn](mailto:huangwenquan@ctgu.edu.cn); Peng Geng, [gengpeng@ctgu.edu.cn](mailto:gengpeng@ctgu.edu.cn)

<sup>†</sup> Wei Wang and Yuting Zhang contribute equally

## CITATION

Wang W, Zhang Y, Li Y, et al. Preparation of cuttlefish ink-porphyrin nanoconjugates and its application in photodynamic-photothermal synergistic treatment of tumor cells. *Nano and Medical Materials*. 2024; 4(1): 1895. <https://doi.org/10.59400/nmm.v4i1.1895>

## ARTICLE INFO

Received: 30 October 2024

Accepted: 13 November 2024

Available online: 5 December 2024

## COPYRIGHT



Copyright © 2024 by author(s).

*Nano and Medical Materials* is published by Academic Publishing Pte Ltd. This work is licensed under the Creative Commons Attribution (CC BY) license.

<https://creativecommons.org/licenses/by/4.0/>

**Abstract:** Biologically derived nanomaterials have gained increasing attention in tumor diagnosis and treatment due to their inherent biocompatibility. In this study, a nanoconjugate of cuttlefish ink (M, extracted from cuttlefish ink sacs) and meso-tetra (4-carboxyphenyl) porphyrin (TCPP), termed M-TCPP, was synthesized. The nanoparticle size of M-TCPP was approximately 120 nm, and it could be activated by a 660 nm light to induce the generation of reactive oxygen species (ROS) via TCPP for photodynamic therapy (PDT) of tumor cells. Additionally, when triggered by an 808 nm light (near-infrared light), the cuttlefish ink component efficiently converted light into heat for photothermal therapy (PTT) of tumor cells. Compared to standalone PDT or PTT, the synergistic combination of PDT-PTT resulted in significantly enhanced tumor cell destruction. Moreover, *in vitro* experiments demonstrated that M-TCPP exhibited no noticeable toxic side effects. The research offers some inspiration for the development of natural multifunctional biomaterials and their use in tumor therapy.

**Keywords:** biomaterials; cuttlefish ink; photodynamic therapy; photothermal therapy; tumor cell

## 1. Introduction

The malignant tumors represent a significant risk to human health. In addition to traditional treatment methods, researchers have been exploring various new treatment technologies in recent years. These mainly include photodynamic therapy (PDT) [1], photothermal therapy (PTT) [2], sonodynamic therapy (SDT) [3], and chemo dynamic therapy (CDT) [4]. However, tumor development and progression are highly intricate, and no single treatment approach fully addresses all clinical requirements [5,6]. As a result, researchers are attempting to combine different therapies to achieve a synergistic “1 + 1 > 2” effect [7,8]. To date, several combination treatment strategies have emerged, such as PDT-PTT [9,10], SDT-PTT [11,12], SDT-PDT [13,14], PDT-CDT [15,16], PDT-chemotherapy [17,18], and PTT-chemotherapy [19,20]. It is worth noting that among the phototherapy combinations (PTT and PDT), PTT is considered an effective treatment method due to its oxygen-independent mechanism and high spatial-temporal precision [21]. PTT typically uses a photothermal agent to trigger localized hyperthermia under near-infrared (NIR) light irradiation, leading to the irreversible ablation of tumor cells with high treatment efficiency [22]. In PDT, laser irradiation at a specific wavelength activates the photosensitizer, which transfers

energy to nearby oxygen molecules, producing ROS that exhibit strong cytotoxicity, leading to cellular damage or death [23]. When PTT and PDT are used in combination, PTT disrupts the membrane structure of cancer cells, enhancing the permeability of ROS into tumor cells, thus improving PDT efficacy. Meanwhile, ROS generated during PDT can disrupt heat shock proteins, which typically prevent DNA denaturation and apoptosis. This disruption enhances the effectiveness of PTT, creating a synergistic effect that complements PDT [24]. The combined PTT-PDT strategy has proven to be effective, as it accelerates blood flow, increases tumor cell oxygenation, promotes ROS generation, and improves the thermosensitivity of tumor cells [25,26]. The key to synergistic PDT-PTT lies in developing new nanomaterials with significant photothermal and photodynamic properties [27]. Several multifunctional nanomaterials have been developed so far for the combined treatment of tumor cells using PDT and PTT.

There are three main strategies for constructing PDT-PTT combinations. The first involves designing inorganic photosensitizers and inorganic photothermal nanomaterials, with gold, iron, copper, tungsten, and molybdenum-based nanomaterials being the most common photothermal and photodynamic agents [28]. However, one of the main challenges of inorganic nanomaterials is their potential toxicity. Over time, inorganic nanomaterials would accumulate in the body, and due to their slow degradation/metabolism, they may cause unwanted side effects/toxicity. The second strategy involves encapsulating organic photosensitizers within inorganic photothermal shells, or vice versa [29]. For example, H-TiO<sub>2</sub>@PDA@ICG (indocyanine green) [30] and Fe<sub>3</sub>O<sub>4</sub>/SiO<sub>2</sub>@CUR (curcumin) [31] composite nanoagents have demonstrated significant photothermal and photodynamic effects. However, the inorganic part of these materials is difficult to degrade in the body, and the organic part is not effectively/rapidly released from the inorganic part, resulting in low utilization efficiency. To address these challenges, a series of organic photothermal-organic photosensitizer nanocomposites have been developed, such as ML880 [32] and DPP-TPA (triphenylamine) [33]. However, organic small molecules generally exhibit poor loading efficiency, and their drug release is uncontrollable. Furthermore, the limited diffusion distance (< 20 nm) of ROS produced by photosensitizers directly leads to poor utilization efficiency of ROS within composite nanoagents [34,35]. Thus, the development of novel organic PDT-PTT nanoagents with optimal ROS diffusion range, along with enhanced biocompatibility and biodegradability, is essential.

Natural melanin is widely distributed in many organisms such as human skin/hair, plant seeds and ink sacs of cuttlefish, which contain active chemical units (such as 5,6-dihydroxyindole-2-carboxylic) with rich amine groups. Cuttlefish ink (M) has been recognized as an excellent agent for PTT of tumors because of their native biocompatibility and biodegradability, which could alleviate safety concerns and default metabolism in biological systems [36]. Additionally, cuttlefish ink contains abundant amino groups, which can undergo amide reactions with photosensitizers containing carboxyl groups to create multifunctional nanoagents [37]. TCPP (meso-tetra (4-carboxyphenyl) porphyrin) is an organic molecule with carboxyl groups and has been recognized as an effective photosensitizer in clinical trials over the years [38]. Moreover, given the short diffusion distance of ROS, TCPP is uniformly distributed

on the surface of M, maximizing the utilization of ROS. In this study, M and TCPP were conjugated through an amide reaction to form the M-TCPP nanoconjugate. M-TCPP exhibited high PDT efficiency and photothermal effects, making it a promising PDT-PTT nanoagent for synergistic tumor cell therapy (**Figure 1**).

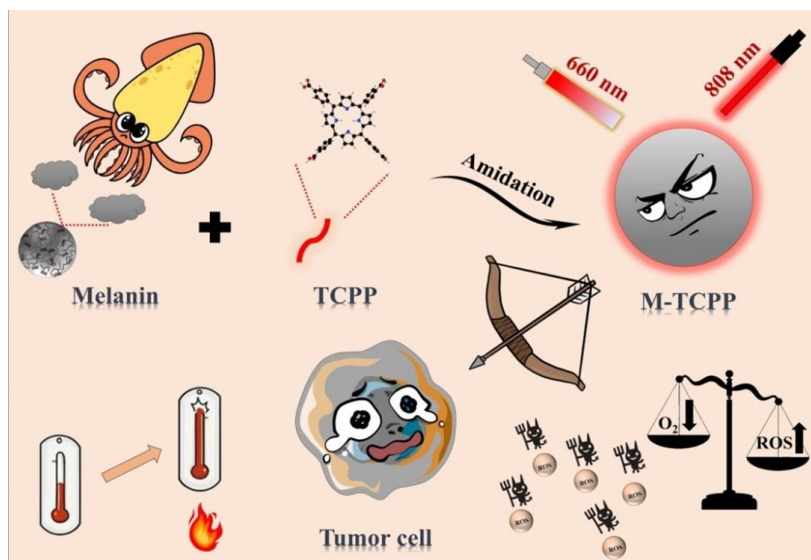


**Figure 1.** A diagram depicting the design of M-TCPP and its application in synergistic PDT-PTT for tumor treatment.

## 2. Materials and methods

### 2.1. Preparation of M-TCPP

First, a specific amount of TCPP (5 mg), EDC (40 mg), and NHS (20 mg) was weighed using an electronic analytical balance and dispersed in 5 mL of DMF solution, stirred in the dark for 2 h. Then, 10 mg of cuttlefish ink was added to the mixture and stirred with a magnetic stirrer for an additional 12 h. Finally, the mixture was centrifuged at 10,000 rpm for 5 min and washed three times with a water/ethanol mixture (1/4 mL).

### 2.2. Singlet Oxygen ( $^1\text{O}_2$ ) Experiment

DPBF (20  $\mu\text{L}$ , 2.0 mg/mL in DMF) was added to the DMF solution of M-TCPP (3 mL, 50 mg/mL), forming a homogeneous mixture. This mixture was then exposed to a light source (660 nm, 0.1  $\text{W}/\text{cm}^2$ ) and labelled as “M-TCPP + DPBF + Light.” The UV-visible absorption spectra were recorded to detect the ROS generation efficiency of M-TCPP during photodynamic therapy. Control experiments were conducted under the same conditions for “DPBF + Light” and “M-TCPP + Light,” and their absorbance changes were also recorded.

### 2.3. Photothermal effect experiment

M-TCPP dispersions at different concentrations (0, 0.025, 0.05, 0.1, and 0.2 mg/mL, 100  $\mu\text{L}$  each) were placed into plastic tubes (150  $\mu\text{L}$ ) and exposed to an 808 nm near-infrared laser (1.0  $\text{W}/\text{cm}^2$ ) for 10 min. Temperature changes were recorded using an infrared thermal imaging camera.

## 2.4. *In vitro* cell experiment

Human umbilical vein endothelial cells (HUVEC) and mouse breast cancer cells (4T1) were cultured in 96-well plates under standard conditions. After 24 h, the culture medium was replaced with a fresh medium containing different concentrations of M-TCPP. Following an additional 24-h incubation, the cells were rinsed with PBS, and cell viability was assessed using the standard MTT assay.

## 3. Results and discussion

### 3.1. Synthesis and characterization of M-TCPP

As shown in (Figure 1), TCPP is an organic molecule with carboxyl groups, commonly used as a photosensitizer in photodynamic therapy (PDT). Cuttlefish ink (M) is a natural biopolymer abundant in amine groups, making it an outstanding photothermal agent for photothermal therapy (PTT). The M-TCPP composite nanoparticles were synthesized by coupling the carboxyl groups of TCPP with the amine groups of cuttlefish ink, enabling their use in combined PDT-PTT therapy. Scanning electron microscopy (SEM) was employed to study the morphology of M-TCPP, which revealed that M-TCPP formed nanoscale microspheres with an average particle size of  $\approx 120$  nm (Figures 2a,b). The optical properties of M-TCPP were then measured using UV-vis spectrophotometry. M exhibited significant absorption in the 300–800 nm range, whereas TCPP showed a distinct absorption peak at 410 nm. The absorption spectrum of M-TCPP exhibited all the characteristic peaks of both TCPP and M, indicating successful coupling. Notably, a slight redshift in peak position was observed in M-TCPP compared to pure TCPP, likely due to energy transfer between TCPP and squid ink (Figure 2c). The interaction between TCPP and carboxyl groups, as well as cuttlefish ink and amine groups, was investigated using Fourier infrared spectroscopy (FTIR) (Figure S1). The FTIR spectra revealed that the amino peak in cuttlefish ink corresponds to the bending vibration of N-H at  $1620\text{ cm}^{-1}$  and the stretching vibration of C-N at  $1368\text{ cm}^{-1}$ . Moreover, M-TCPP exhibited two new carboxylic acid bands at  $1690\text{ cm}^{-1}$  and  $1400\text{ cm}^{-1}$ , while TCPP did not display any carboxylic acid stretching bands ( $1688\text{ cm}^{-1}$ ), indicating the presence of -CONH- groups. Moreover, when excited at 560 nm, TCPP in DMF solution displayed its primary emission peak at 660 nm. In contrast, the fluorescence intensity of M-TCPP was notably lower than that of TCPP, suggesting an energy transfer from TCPP to M. (Figure 2d). This confirms the successful conjugation of TCPP onto the surface of squid ink. Additionally, the average hydrodynamic size of M-TCPP was found to be  $\approx 165$  nm (Figure 2e). The surface of cuttlefish ink carries a negative charge [39], and the Zeta potential shifts from  $-10.7$  mV for TCPP to  $-17.9$  mV for M-TCPP (Figure 2f), further confirming the successful conjugation of TCPP on the cuttlefish ink surface [29].

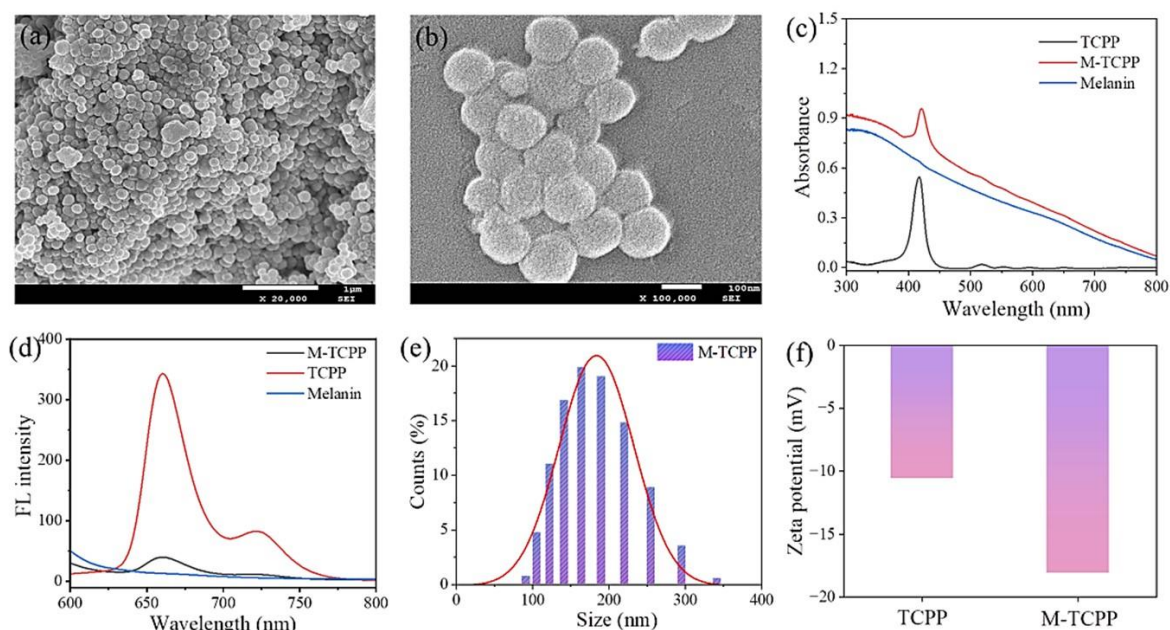


**Figure 2.** (a, b) SEM images of M-TCPP; UV-vis absorption spectra; (c) and fluorescence spectra; (d) of M-TCPP, TCPP and cuttlefish ink; (e) Hydrodynamic dimensions of the M-TCPP; (f)  $\zeta$ -potential for TCPP and M-TCPP.

### 3.2. Photodynamic effect of M-TCPP

The M-TCPP nanocomposite was formed by coupling TCPP with cuttlefish ink, where the TCPP component can be excited by a 660 nm light source to convert  $O_2$  into cytotoxic singlet oxygen ( $^1O_2$ ). The production of  $^1O_2$  was detected using 1,3-diphenylisobenzofuran (DPBF) as an indicator (**Figure 3a**). When the mixture of M-TCPP and DPBF was exposed to light for 5 min, the characteristic absorption peak of DPBF at 415 nm rapidly decreased with increasing light exposure time, indicating that  $^1O_2$  was generated by the (M-TCPP + DPBF + Light) system (**Figure 3b**). To rule out other possible influences, we also tested the absorbance changes of the pure DPBF group and the M-TCPP group under the same conditions. It was found that 34.1% of the DPBF was oxidized in the M-TCPP + Light (5 min) group, whereas there was no significant reduction in absorbance in either the pure DPBF or M-TCPP groups (**Figure 3c**). These results demonstrate that M-TCPP can effectively generate  $^1O_2$  under 660 nm light irradiation, showing potential for application in PDT.

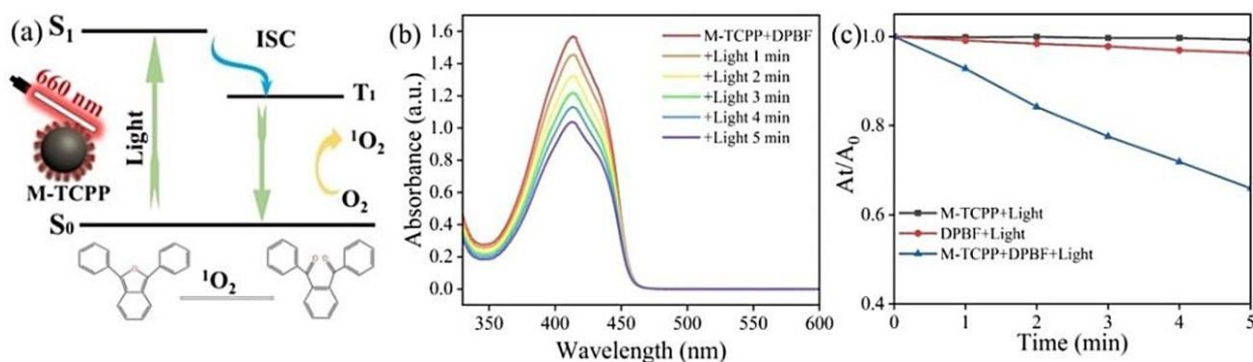


**Figure 3.** (a) Schematic diagram of M-TCPP stimulated by Light to produce  $^1O_2$  and oxidize DPBF; (b) UV-vis absorption spectra of M-TCPP + DPBF + Light with time variation; (c) Under the same conditions, the absorbance changes of different test groups.

### 3.3. Photothermal effect of M-TCPP

With the increase in M-TCPP concentration (ranging from 0.025 to 0.2 mg/mL), the optical absorption of the M-TCPP dispersions was significantly improved (**Figure 4a**). When subjected to an 808 nm laser ( $1.0 \text{ W/cm}^2$ ), these dispersions demonstrated a rapid rise in temperature in response to laser irradiation, indicating a strong photothermal effect that depended on concentration. At concentrations of 0, 0.025, 0.05, 0.1, and 0.2 mg/mL, the temperature elevations of the M-TCPP dispersions were  $5.8 \text{ }^\circ\text{C}$ ,  $12.5 \text{ }^\circ\text{C}$ ,  $19.5 \text{ }^\circ\text{C}$ ,  $30.8 \text{ }^\circ\text{C}$ , and  $47.5 \text{ }^\circ\text{C}$  respectively (**Figure 4b**). The temperature increase of M-TCPP dispersion ( $0.1 \text{ mg} \cdot \text{mL}^{-1}$ ) was  $10.5 \text{ }^\circ\text{C}$ ,  $17.6 \text{ }^\circ\text{C}$ ,  $25.2 \text{ }^\circ\text{C}$ ,  $30.8 \text{ }^\circ\text{C}$ , and  $37.3 \text{ }^\circ\text{C}$  at laser powers of  $0.3, 0.6, 0.8, 1.0$  and  $1.3 \text{ W/cm}^2$  respectively (**Figure S3**). Infrared thermal images of the M-TCPP ( $0.1 \text{ mg/mL}$ ) dispersion demonstrated a gradual increase in thermal imaging signal intensity with extended 808 nm laser irradiation, indicating that M-TCPP possesses an excellent photothermal conversion effect (**Figure 4c**). After four photothermal cycles, the photothermal conversion effect of the M-TCPP ( $0.1 \text{ mg/mL}$ ) dispersion was well-maintained (**Figure 4d**), suggesting good photothermal cycle stability. The photothermal conversion efficiency of M-TCPP was calculated to be 31.5% (**Figure 4e**). Additionally, the photothermal performance of M-TCPP in PBS solution ( $0.1 \text{ mg} \cdot \text{mL}^{-1}, 1.0 \text{ W} \cdot \text{cm}^{-2}$ ) was tested over some time. The results showed that M-TCPP exhibited a similar photothermal effect after a 48-h interval in PBS solution, further demonstrating its excellent long-term photothermal stability (**Figure S4**). In summary, M-TCPP nanocomposite exhibits excellent photothermal conversion efficiency, highlighting its promising potential for applications in photothermal therapy (PTT).

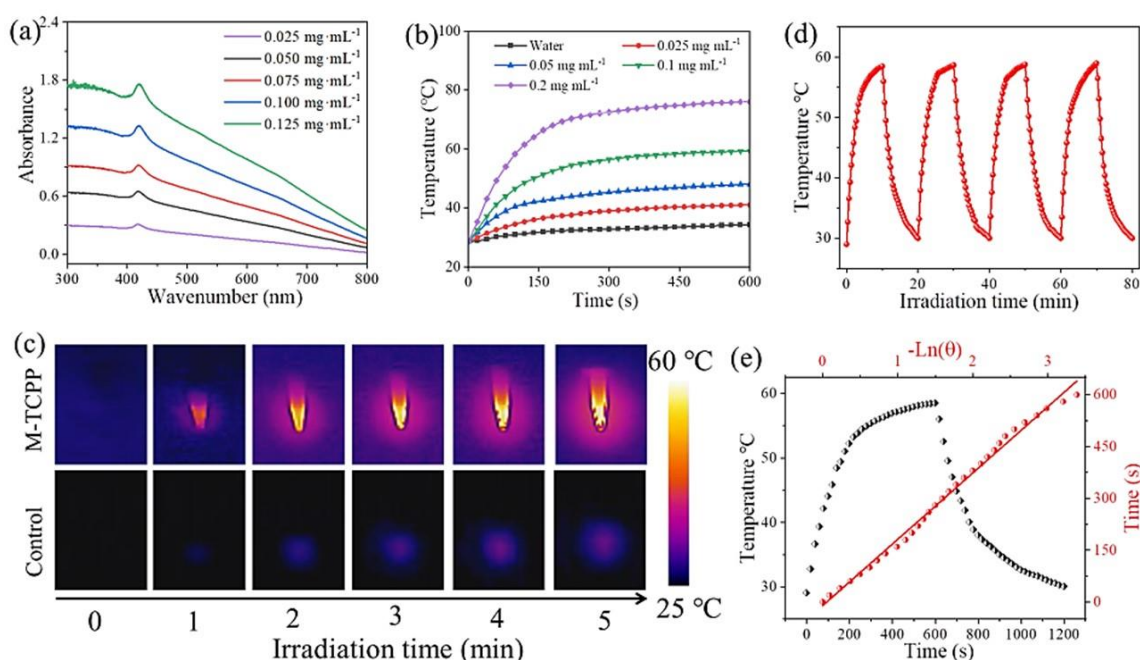


**Figure 4.** (a) UV-vis absorption spectra of M-TCPP with different concentrations; (b) temperature rise curves of different concentrations of M-TCPP; (c) photothermal imaging of M-TCPP; (d) temperature changes of M-TCPP over four irradiation cycles; (e) temperature curve of M-TCPP moisture dispersion after 808 nm laser on/off and linear time data with  $-\ln(\theta)$  after NIR laser off.

### 3.4. Cytotoxicity and *in vitro* photodynamic-photothermal combination therapy

To assess the biocompatibility of M-TCPP, M-TCPP was co-incubated with HUVEC and 4T1 cells for 24 h, and cell viability was measured using the MTT assay. The results showed that after 24 h of co-incubation, the cells remained highly viable, with an average survival rate of over 88% at a concentration of 0.4 mg/mL, confirming the good biocompatibility of M-TCPP (Figures 5a,b). Next, the uptake of M-TCPP (0.2 mg/mL) by 4T1 cancer cells was investigated. Under identical experimental conditions, ink from squid served as a non-fluorescent control. After 4 h of co-incubation with M-TCPP, strong red fluorescence was observed in 4T1 cells, indicating that M-TCPP was effectively taken up/endocytosed by the 4T1 cells (Figure 5c).

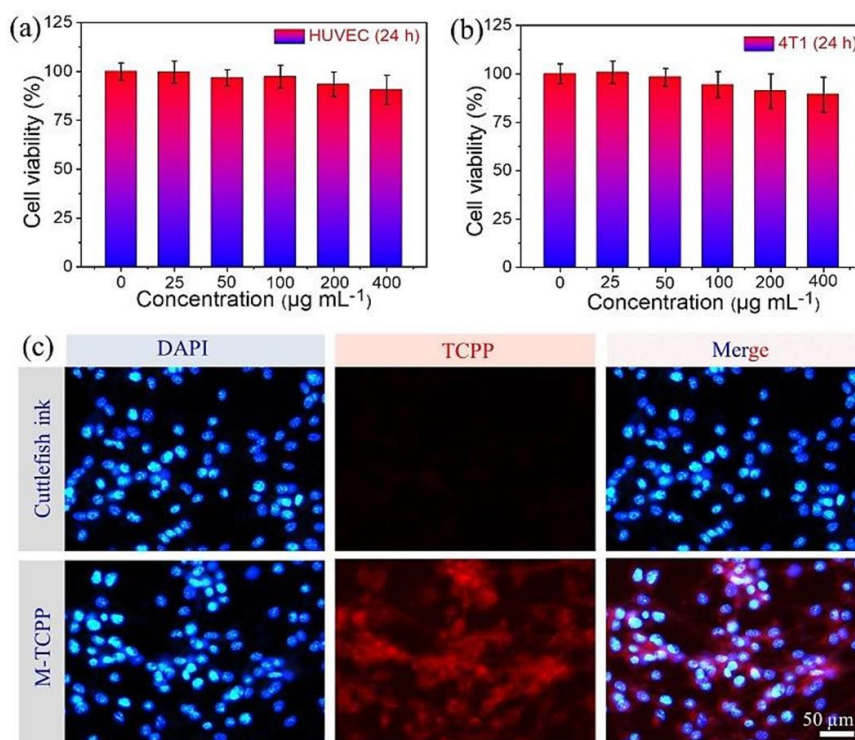


**Figure 5.** (a, b) Cytotoxicity of HUVEC and 4T1 cells under different concentrations of M-TCPP; (c) Fluorescence images of 4T1 cells after incubation with M-TCPP or M for 4 h.

Next, the PDT and PTT effects of M-TCPP on 4T1 tumor cells were studied *in vitro*. 4T1 cells were incubated with M-TCPP (0.2 mg/mL) for 12 h, followed by irradiation with either 808 nm laser (NIR) or 660 nm laser (Light) in some groups (Figure 6a). The cells were divided into seven groups: (1) Control group; (2) M-TCPP group; (3) NIR irradiation group; (4) Light irradiation group; (5) M-TCPP + NIR group; (6) M-TCPP + Light group; and (7) M-TCPP + NIR + Light group. Cell viability in these groups was measured using the MTT assay, and fluorescence microscopy was used to observe cell staining. In groups (1–4), the cell viability remained above 85%, indicating that neither M-TCPP alone nor irradiation with NIR or Light alone had any significant cytotoxic effect on the 4T1 cancer cells. However,

in group (5), the cell viability dropped to 43.1%, demonstrating that M-TCPP under NIR irradiation exhibited effective PTT performance. Furthermore, in group (6), the cell viability decreased to 56.2%, confirming the efficacy of PDT. Most importantly, the lowest cell viability was observed in group (7), with a survival rate of only 16.8%, attributed to the strong synergistic effect of PTT-PDT combination therapy (**Figure 6b**). Fluorescence microscopy images further supported these results, showing predominantly green fluorescence (live cells) in groups (1–4). In contrast, groups (5–7) exhibited a decrease in green fluorescence and a corresponding increase in red fluorescence (dead cells), indicating reduced cell viability. Notably, group (7) (M-TCPP + NIR + Light) displayed the highest number of red fluorescent (dead) cells (**Figure 6c**). In summary, the combination of M-TCPP with both 808 nm and 660 nm laser irradiation demonstrated excellent photothermal-photodynamic synergistic effects, effectively killing tumor cells.

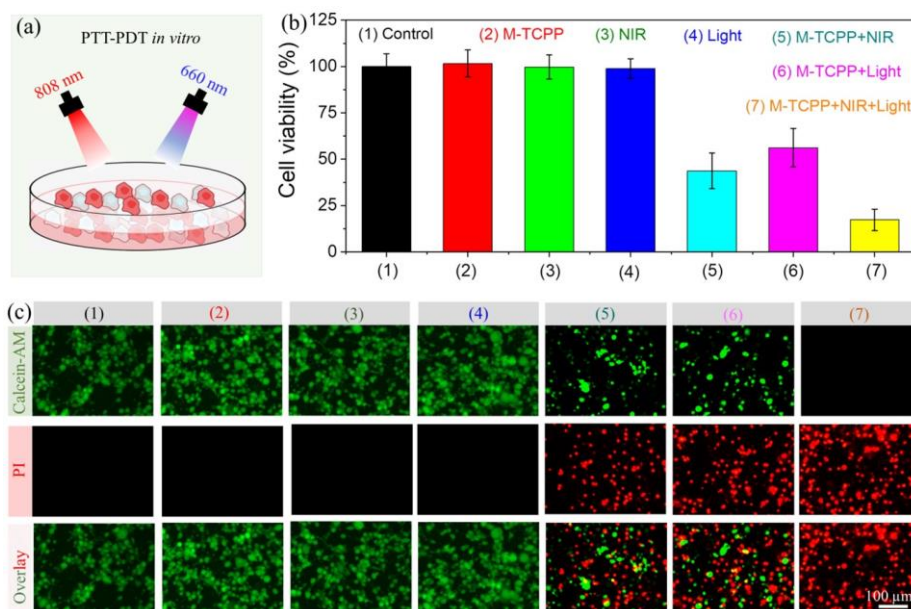


**Figure 6.** (a) Schematic diagram of combined PTT-PDT *in vitro*. Relative survival rate; (b) and fluorescence image; (c) of 4T1 cells treated in different groups.

#### 4. Conclusions

In summary, a biomimetic M-TCPP nanomaterial was successfully synthesized by coupling TCPP with cuttlefish ink. M-TCPP demonstrated efficient production of ROS under 660 nm laser irradiation and rapid heat generation under 808 nm laser irradiation, exhibiting excellent photodynamic and photothermal effects. Additionally, M-TCPP displayed good biocompatibility, and its combined PDT-PTT treatment significantly enhanced the ability to kill tumor cells compared to PDT or PTT alone. This study provides a promising new strategy for tumor cell treatment using biocompatible materials.

**Supplementary materials:** Experimental materials and instruments, FTIR spectra, XRD spectra, photothermal effect under different laser power, and stability assessment are provided in the Supporting Information.

**Author contributions:** Conceptualization, PG and SX; methodology, PG and WH; formal analysis, PG and WW; investigation, WW, YZ, YL and YH; experiment, WW and YZ; writing—original draft preparation, WW; writing—review and editing, PG and WW; funding acquisition, PG, SX and WH. All authors have read and agreed to the published version of the manuscript.

**Acknowledgment:** We are grateful for the financial support from the National Natural Science Foundation of China (22171163), the Natural Science Foundation of Hubei Province (2024AFB059), the 111 Project (D20015), and the Yichang Natural Science Research Program (A23-2-025).

**Conflict of interest:** The authors declare no conflict of interest.

## References

1. Zhao M, Zhuang H, Li B, et al. In Situ Transformable Nanoplatfoms with Supramolecular Cross-Linking Triggered Complementary Function for Enhanced Cancer Photodynamic Therapy. *Advanced Materials*. 2023; 35(20): e2209944. doi: 10.1002/adma.202209944
2. Liu Y, Luo Y, Gao Y, et al. Carrier-Free Biomimetic Organic Nanoparticles with Super-High Drug Loading for Targeted NIR-II Excitable Triple-Modal Bioimaging and Phototheranostics. *Small*. 2024; e2406003. doi: 10.1002/smll.202406003
3. Gao F, He G, Yin H, et al. Titania-coated 2D gold nanoplates as nanoagents for synergistic photothermal/sonodynamic therapy in the second near-infrared window. *Nanoscale*. 2019; 11(5): 2374–2384. doi: 10.1039/c8nr07188h
4. Yu J, Yan H, Zhao F, et al. Intraparticle Electron Transfer for Long-Lasting Tumor Chemodynamic Therapy. *Advanced Science*. 2024; 11(36): e2403935. doi: 10.1002/advs.202403935
5. Li C, Pang Y, Xu Y, et al. Near-infrared metal agents assisting precision medicine: From strategic design to bioimaging and therapeutic applications. *Chemical Society Reviews*. 2023; 52(13): 4392–4442. doi: 10.1039/d3cs00227f
6. Bindra A, Wang D, Zhao Y. Metal-Organic Frameworks Meet Polymers: From Synthesis Strategies to Healthcare Applications. *Advanced Materials*. 2023; 35(40): e2300700. doi: 10.1002/adma.202300700
7. Geng P, Yu N, Macharia D, et al. MOF-derived CuS@Cu-MOF nanocomposites for synergistic photothermal-chemodynamic-chemo therapy. *Chemical Engineering Journal*. 2022; 441: 135964. doi:10.2139/ssrn.4013479
8. Zhang M, Liu X, Luo Q, et al. Tumor environment responsive degradable CuS@mSiO<sub>2</sub>@MnO<sub>2</sub>/DOX for MRI guided synergistic chemo-photothermal therapy and chemodynamic therapy. *Chemical Engineering Journal*. 2020; 389: 124450. doi: 10.1016/j.cej.2020.124450
9. Li B, Wang W, Zhao L, et al. Multifunctional AIE Nanosphere-Based “Nanobomb” for Trimodal Imaging-Guided Photothermal/Photodynamic/Pharmacological Therapy of Drug-Resistant Bacterial Infections. *ACS Nano*. 2023; 17(5): 4601–4618. doi: 10.1021/acsnano.2c10694
10. Li L, Li J, Hu R, et al. Tumor Cell Targeting and Responsive Nanoplatfom for Multimodal-Imaging Guided Chemodynamic/Photodynamic/Photothermal Therapy toward Triple Negative Breast Cancer. *ACS Applied Materials & Interfaces*. 2023; 15(23): 27706–27718. doi: 10.1021/acsmi.3c04709
11. Geng P, Xiang G, Zhang W, et al. Hollow copper sulfide loaded protoporphyrin for photothermal-sonodynamic therapy of cancer cells. *Chinese Journal of Inorganic Chemistry*. 2024; 40(10): 1903-1910. doi: 10.11862/CJIC.20240155
12. Han X, Huang J, Jing X, et al. Oxygen-Deficient Black Titania for Synergistic/Enhanced Sonodynamic and Photoinduced Cancer Therapy at Near Infrared-II Biowindow. *ACS Nano*. 2018; 12(5): 4545–4555. doi: 10.1021/acsnano.8b00899
13. Li Y, Wang W, Zhang Y, et al. Design and Synthesis of Nanoscale Zr-Porphyrin IX Framework for Synergistic Photodynamic and Sonodynamic Therapy of Tumors. *Acta Chimica Sinica*. 2024; 82: 443–448. doi: 10.6023/A24010035
14. Geng P, Li Y, Macharia Daniel, et al. One Stone, Three Birds: Design and Synthesis of “All-in-One” Nanoscale Mn-Porphyrin Coordination Polymers for Magnetic Resonance Imaging-Guided Synergistic Photodynamic-Sonodynamic Therapy. *Journal of Colloid and Interface Science*. 2024; 660: 1021–1029. doi: 10.1016/j.jcis.2024.01.157
15. Chin Y, Yang L, Hsu F, et al. Iron oxide@chlorophyll clustered nanoparticles eliminate bladder cancer by photodynamic immunotherapy-initiated ferroptosis and immunostimulation. *Journal of Nanobiotechnology*. 2022; 20(1): 373. doi: 10.1186/s12951-022-01575-7

16. Cheng S, Shi Y, Su C, et al. MnO<sub>2</sub> nanosheet-mediated generalist probe: Cancer-targeted dual-microRNAs detection and enhanced CDT/PDT synergistic therapy. *Biosensors and Bioelectronics*. 2022; 214: 114550. doi: 10.1016/j.bios.2022.114550
17. Geng P, Yu N, Liu X, et al. GSH-Sensitive Nanoscale Mn<sup>3+</sup>-Sealed Coordination Particles as Activatable Drug Delivery Systems for Synergistic Photodynamic-Chemo Therapy. *ACS Applied Materials & Interfaces*. 2021; 13(27): 31440–31451. doi: 10.1021/acsami.1c06440
18. Zhang L, Gao Y, Sun S, et al. pH-Responsive metal-organic framework encapsulated gold nanoclusters with modulated release to enhance photodynamic therapy/chemotherapy in breast cancer. *Journal of Materials Chemistry B*. 2020; 8(8): 1739–1747. doi: 10.1039/c9tb02621e
19. Wang Y, Chen J, Bo Y, et al. Green synthesis of Au nanoparticles by *Scutellaria barbata* extract for chemo-photothermal anticancer therapy. *Pharmacological Research-Modern Chinese Medicine*. 2024; 13: 100536. doi: 10.1016/j.prmcm.2024.100536
20. Li H, Zhu L, Zhang Y, et al. Biomimetic nanotherapeutics for homotypic-targeting photothermal/chemotherapy of oral cancer. *Journal of Controlled Release*. 2024; 366: 28–43. doi: 10.1016/j.jconrel.2023.12.039
21. Liu Y, Zhang J, Zhou X, et al. Dissecting Exciton Dynamics in pH-Activatable Long-Wavelength Photosensitizers for Traceable Photodynamic Therapy. *Angewandte Chemie International Edition*. 2024; 63(43): e202408064. doi: 10.1002/anie.202408064
22. Wang H, Xue K, Yang Y, et al. In Situ Hypoxia-Induced Supramolecular Perylene Diimide Radical Anions in Tumors for Photothermal Therapy with Improved Specificity. *Journal of the American Chemical Society*. 2022; 144(5): 2360–2367. doi: 10.1021/jacs.1c13067
23. Li W, Yang J, Luo L, et al. Targeting photodynamic and photothermal therapy to the endoplasmic reticulum enhances immunogenic cancer cell death. *Nature Communications*. 2019; 10(1): 3349. doi: 10.1038/s41467-019-11269-8
24. Urazaliyeva A, Kanabekova P, Beisenbayev A, et al. All organic nanomedicine for PDT-PTT combination therapy of cancer cells in hypoxia. *Scientific Reports*. 2024; 14(1): 17507. doi: 10.1038/s41598-024-68077-4
25. Wan G, Liu Y, Chen B, et al. Recent advances of sonodynamic therapy in cancer treatment. *Cancer Biology & Medicine*. 2016; 13: 325–338. doi: 10.20892/j.issn.2095-3941.2016.0068
26. Song X, Zhang Q, Chang M, et al. Nanomedicine-Enabled Sonomechanical, Sonopiezoelectric, Sonodynamic, and Sonothermal Therapy. *Advanced Materials*. 2023; 35(31): e2212259. doi: 10.1002/adma.202212259
27. Sheng Y, Ren Q, Tao C, et al. Construction of PEGylated chlorin e6@CuS-Pt theranostic nanoplatfoms for nanozymes-enhanced photodynamic-photothermal therapy. *Journal of Colloid and Interface Science*. 2023; 645: 122–132. doi: 10.1016/j.jcis.2023.04.092
28. Fernandes N, Rodrigues C, Moreira A, et al. Overview of the application of inorganic nanomaterials in cancer photothermal therapy. *Biomaterials Science*. 2020; 8(11): 2990–3020. doi: 10.1039/d0bm00222d
29. Li Y, Huang L, Li X, et al. From biomaterials to biotherapy: cuttlefish ink with protoporphyrin IX nanoconjugates for synergistic sonodynamic-photothermal therapy. *Journal of Materials Chemistry B*. 2024; 12(7): 1837–1845. doi: 10.1039/d3tb02423g
30. Tang W, Kang J, Yang L, et al. Thermosensitive nanocomposite components for combined photothermal-photodynamic therapy in liver cancer treatment. *Colloids and Surfaces B-Biointerfaces*. 2023; 226: 113317. doi: 10.1016/j.colsurfb.2023.113317
31. Ashkbar A, Rezaei F, Attari F, et al. Treatment of breast cancer in vivo by dual photodynamic and photothermal approaches with the aid of curcumin photosensitizer and magnetic nanoparticles. *Scientific Reports*. 2020; 10(1): 21206. doi: 10.1038/s41598-020-78241-1
32. Jin T, Cheng D, Jiang G, et al. Engineering naphthalimide-cyanine integrated near-infrared dye into ROS-responsive nanohybrids for tumor PDT/PTT/chemotherapy. *Bioactive Materials*. 2021; 14: 42–51. doi: 10.1016/j.bioactmat.2021.12.009
33. Cai Y, Liang P, Tang Q, et al. Diketopyrrolopyrrole-Triphenylamine Organic Nanoparticles as Multifunctional Reagents for Photoacoustic Imaging-Guided Photodynamic/Photothermal Synergistic Tumor Therapy. *ACS Nano*. 2017; 11(1): 1054–1063. doi: 10.1021/acs.nano.6b07927
34. Geng P, Yu N, Liu X, et al. One Responsive Stone, Three Birds: Mn (III)-Hemoporphin Frameworks with Glutathione-Enhanced Degradation, MRI, and Sonodynamic Therapy. *Advanced Healthcare Materials*. 2021; 10(3): 2001463. doi: 10.1002/adhm.202001463

35. Geng P, Yu N, Liu X, et al. Sub 5 nm Gd<sup>3+</sup> -Hemoporphin Framework Nanodots for Augmented Sonodynamic Theranostics and Fast Renal Clearance. *Advanced Healthcare Materials*. 2021; 10(18): 2100703. doi: 10.1002/adhm.202100703
36. Qu W, Fan J, Zheng D, et al. Deep-penetration functionalized cuttlefish ink nanoparticles for combating wound infections with synergetic photothermal-immunologic therapy. *Biomaterials*. 2023; 301: 122231. doi: 10.1016/j.biomaterials.2023.122231
37. Zhang J, Shi C, Shan F, et al. From biology to biology: Hematoporphyrin-melanin nanoconjugates with synergistic sonodynamic-photothermal effects on malignant tumors. *Chemical Engineering Journal*. 2021; 408: 127282. doi.org/10.1016/j.cej.2020.127282
38. Meng X, Wu J, Hu Z, et al. Coordinating effect of ferroptosis and in situ disulfiram toxification for enhanced cancer therapy. *Chemical Engineering Journal*. 2024; 484: 149313. doi: 10.1016/j.cej.2024.149313
39. Wang J, Song Z, He M, et al. Light-responsive and ultrapermeable two-dimensional metal-organic framework membrane for efficient ionic energy harvesting. *Nature Communication*. 2024; 15(1): 2125. doi: 10.1038/s41467-024-46439-w